ADVANCES IN SURFACE ENGINEERING

Properties and High-Temperature Wear Behavior of Remelted NiCrBSi Coatings

ALİ GÜNEN [1,2,3] and AHMET ÇÜRÜK [1]

1.—Department of Metallurgy and Materials Engineering, Faculty of Engineering and Natural Sciences, Iskenderun Technical University, 31200 Hatay, Turkey. 2.—e-mail: ali.gunen@iste.edu.tr. 3.—e-mail: aligunen2013@gmail.com

Remelted NiCrBSi coatings were examined using optical microscopy, scanning electron microscopy, energy dispersive spectroscopy, x-ray diffraction analysis, microhardness and wear testing. After wear tests, the surfaces of the worn samples were examined by 3D profilometry and scanning electron microscopy to investigate the effects of load and temperature on the coefficient of friction and wear resistance. In all the wear experiments, there was a momentary increase in the wear volume and a momentary decrease in the average coefficient of friction values at the elevated test temperatures. This behavior was caused by the stable oxide layer formed on the surface as a consequence of the elevated test temperature. Three dominant wear mechanisms were observed with the NiCrBSi coatings: delamination at room temperature, spalling and adhesion at 250°C, and oxidation at 450°C, whereas in the uncoated samples there was delamination at room temperature, and micro-cracking and oxidation, both at 250°C and 450°C. Remelted NiCrBSi coatings provided better wear resistance and lower coefficient of friction than uncoated STKM-13A steel, especially at higher temperatures.

INTRODUCTION

Hot-rolling is an important process in the iron and steel industry due to its many advantages, including the refinement of the grains, elimination of the defects of the microstructure, easier formability, and continuous production.[1] Ideally, roll materials should have superior surface quality, higher hardness than the material to be rolled, and should be resistant to elevated temperatures, thermal-shock, cracking, and wear.[2–5] However, producing an alloy with all of these properties would be very costly. Instead, it is more economical and practical to use post-processing, specifically coatings, to provide some of these properties.[6] Indeed, hard ceramic and composite coatings have shown significant progress in recent years in the rolling mills.[2–7]

The most widely accepted methods for coating surfaces for rolling mills are physical vapor deposition (PVD),[3,8] laser cladding,[9,10] chemical vapor deposition (CVD),[11] vacuum-arc deposition,[12] and thermal spraying (TS).[13–15] TS is the most commonly used methods in industry as it allows easier, faster, and more economical coatings with greater thickness as compared to other methods such as CVD, PVD, laser cladding, etc.[16]

During TS, metallic, ceramic, and cermet materials are heated to form semi-molten or molten particles that are subsequently sprayed as atomized jets onto a previously prepared substrate. On the substrate surface, adhered particles form a layered structure and cool down due to the heat transfer from the particles to the substrate.[16,17] Flame spray coating is one of the most widely used variant of TS due to its ease of applicability and economic efficiency. However, it has disadvantages, such as high porosity, oxide interlayer formation, and poor adhesion to the substrate.[13,16,17] These disadvantages, fortunately, can be overcome by a subsequent remelting process, the most frequently used ones being flame,[18–23] furnace,[23–25] and laser[18,19,22,23] remelting. The thermal post-treatments lead to the elimination of some unwelcome coating features (i.e., pores, oxides, and unmelted particles), and create a metallurgical bond between the coating and the substrate.[17,25–27]

A coating of NiCrBSi is common in rolling materials that are to be used under conditions where wear and corrosion are important

considerations.[19,27,28] Cr and Ni grant improved corrosion resistance, and the silicides, borides and borocarbides, that are formed enhance the wear resistance of the substrate. Moreover, the presence of B and Si in the powder protect other elements from oxidation by forming borosilicate and also improve the wettability during the deposition process.[25]

Although NiCrBSi coatings have enjoyed wide use at high temperatures, most previous studies have investigated their microstructure, mechanical and corrosion behavior at room temperature.[18–20,22,25–28] There are only a limited number of studies at high temperatures. Chaliampalias et al.[29] carried out a comparative study on the microstructure and high-temperature oxidation performance of flame-sprayed NiCrBSi coatings and pack cementation coatings. They reported that the pack cementation coatings exhibited better properties than the flame-sprayed coatings in terms of homogeneity, porosity, hardness, adhesion, and oxidation resistance, although they had a lower coating thickness. Karimi et al.[26] investigated the effect of remelting on the porosity and the characteristics of pore shape and pore size of flame-sprayed NiCrBSi coatings, and they claimed that remelting resulted in an approximate 6-fold decrease in porosity and enhanced the metallurgical bonding between the coating and the substrate. They also pointed out that the microstructure of the coating depended on the substrate material, the fusing temperature, and the sample dimensions. Also, due to the high rate of deposition and cooling, flame-sprayed coatings are far from the thermodynamic equilibrium, and different conclusions can be obtained even for similar conditions. Simunovic et al.[27] studied the flame spraying and fusing of NiCrBSi, NiCrWBSi and NiCrBSi + tungsten-carbide (WC) powder on C45, 42CrMo4, and X6CrNiMo18-10-2 steels. They stated that the temperature of the remelting stage has a great influence on the modified surface and the sample dimensions on the substrate. The most striking finding in their work was that different conclusions could be drawn from similar conditions, since TS coatings are far from the thermodynamical equilibrium state due to high rates of deposition and cooling. Liang et al.[20] compared remelted flame-sprayed NiCrBSi coatings in terms of microstructure and wear resistance, and stated that induction remelting provides high hardness, excellent wear resistance, and better remelting quality than the flame remelting process.

NiCrBSi coatings have also been reported in many studies where they are used in advanced engineering fields, such as aircraft construction, and in the aerospace and petro-chemical industries due to their high wear[14,15] and oxidation resistance.[19,29] A few studies are available for the wear behavior of NiCrBSi coatings at high temperatures, deposited by, for instance, plasma spraying,[21,30] high velocity oxygen fuel (HVOF),[31] and laser

cladding.[32] To the authors' knowledge, there exists only one publication examining the wear resistance of flame-sprayed NiCrBSi coating at an elevated temperature (500°C), but without a further flame remelting treatment.[21] Load is also stated to be more influential than temperature on the wear characteristics of NiCrBSi.[21] Wear test loads applied on flame-sprayed combined with flame-remelting NiCrBSi coatings range, in the literature, between 10 N and 450 N.[14,18,19,22,23] Externally cooled rolls, the principle application for the current study, are generally subjected to temperatures of 250–450°C and loads of 1–3 N.[33] Therefore, in the present work, coatings of a NiCrBSi self-fluxing alloy were deposited on a STKM-13A steel substrate by flame spray with a subsequent flame treatment. The high-temperature (250°C and 450°C) friction and wear behavior of the grown coatings was comparatively investigated under relatively low loads (1 and 3 N) by means of a pin-on-plate dry sliding wear tester. Coating microstructures and the responsible wear mechanism were also identified.

MATERIALS AND METHODS

STKM-13A (0.9 wt.% Mn, 0.25 wt.% C, 0.35 wt.% Si, 0.04 wt.% P, 0.04 wt.% S, balance Fe) was used as the substrate material, with specimen dimensions of $70 \times 70 \times 5$ mm. A spectral analyzer (DV-6S 3063A; Thermo Jarrell ASH-BAIRD, USA) was used for chemical analysis. Commercial Metco 15F (a self-fluxing powder containing 17 wt.% Cr, 4 wt.% Si, 4 wt.% Fe, 3.5 wt.% B, 1 wt.% C, balance Ni) was used as the coating powder in the flame spray process. The flame-sprayed samples were cleaned and grit-blasted with Al_2O_3 grade 36 with four passes. A spray distance of 150 mm, a powder feed rate pressure of 10 kg/h, a C_2H_2 flow rate of 1.0 m^3/h and O_2 flow rate of 1.5 m^3/h were selected as process parameters for the flame spraying, which was carried out using a Metco type 5P spray gun. Then, the samples were subjected to remelting by flame treatment at 1050°C to obtain better mechanical properties. The process parameters for remelting by flame were selected as a C_2H_2 flow rate of 1.0 m^3/h and O_2 flow rate of 1.5 m^3/h with constant fire. Thermocouples were placed on the surface of the samples and when the sample reached 1050°C, this was held for 10 min and then the samples were cooled to room temperature in the open air.

Specimens for metallography, microhardness and x-ray diffraction (XRD) were cut to a size of $10 \times 10 \times 5$ mm. The metallography specimens were sectioned and cold-mounted. The specimens were then ground using 400, 600, 800, 1000 and 1200 grit abrasive papers and polished with 3-μm alumina paste followed by 1-μm diamond paste. After polishing, the specimens were etched with a solution consisting of 4 wt.% Nital for 1 min to reveal the microstructural details. Optical

microscopy was carried out using a metal microscope (Eclipse MA-200; Nikon, Japan) equipped with a digital image analysis system (Clemex, Clemex Technologies, Canada). Scanning electron microscopy (SEM) studies were performed with a scanning electron microscope (Oxford X-Max, UK) equipped with energy dispersive spectroscopy (EDS) capability, at 50 kV accelerating voltage. Porosity measurements were carried out as detailed in Ref. 25. Microhardness measurements of the layers were conducted utilizing a hardness tester (Highwood HWMMT-X3; TTS Unlimited, Japan) with a Vickers pyramid indenter along the cross-section using a 100-g load and a 15-s dwell time. The coating thickness was measured using the Clemex system which was connected to the Nikon MA-200 optical microscope. Values of the thickness and hardness were averaged from ten and five measurements, respectively. XRD analyses were carried out using a computer-controlled Bruker AXS D8 Advance Diffractometer with CuK$_\alpha$ radiation (λ_{Cu} = 0.1540 nm) and 2θ angles ranging from 0° to 90°.

Dry sliding wear and friction tests of untreated or NiCrBSi flame-sprayed STKM-13A steel (70 × 70 × 5 mm) against a WC abrasive ball (diameter 6 mm, hardness 19 GPa) were carried out in a temperature-controlled ball-on-disk tribometer (T10/20; Turkyus Tribometer, Turkey) under atmospheric conditions. The friction force at the articulating interface was detected by a load cell through a friction force measurement arm, from which the friction coefficient (COF) (the ratio of the friction force to compressive load) was calculated. Wear test conditions were determined using data collected from externally cooling rolls in actual working conditions, as stated in our previous study.[8,33] Therefore, the tests were carried out under 1 N or 3 N loading, at 5 mm stroke length, at 0.3 m/s sliding speed, for 270 m total sliding distance, under dry sliding conditions, and at 25°C, 250°C or 450°C. The contact areas between the WC ball and the flame spray coating was measured using super high pressure sensitive film (Fuji Photo Film, Tokyo, Japan), as stated in the previous study.[34] The average contact pressures were calculated by
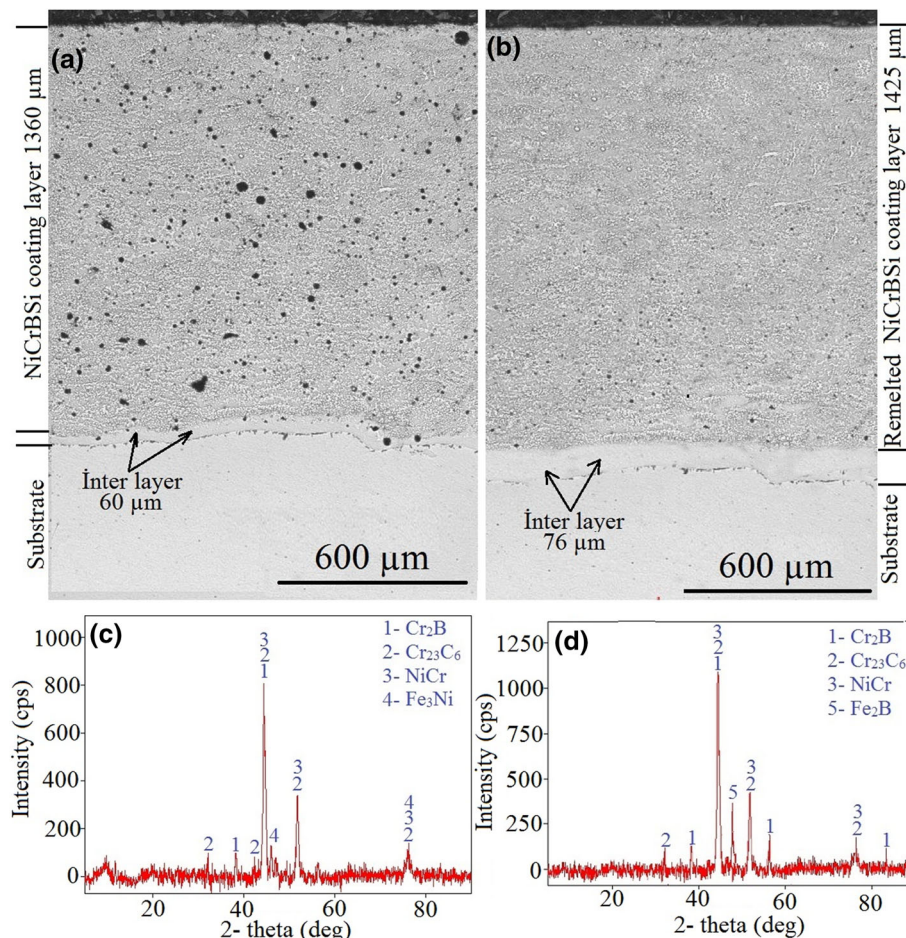

Fig. 1. Cross section of optical appearances of NiCrBSi coating sample: (a) unmelted (b) remelted, and XRD analysis of (c) unmelted (d) remelted NiCrBSi samples.

dividing the static loads of 1 and 3 N into the contact areas. The average contact pressures were calculated as 1.7–1.8 GPa and 2.0–2.1 GPa for the 1-N and 3-N load, respectively. Each test was repeated three times and averaged to ensure the accuracy of the test results. Surface roughness of the coatings was reduced by carrying out a final surface finishing step in a lathe to keep it at the desired value [the average surface roughness (R_a) < 5 μm] and thus to improve the service life of the material.[33] The R_a values for the untreated and coated specimens were measured using a 3D optical profilometer (α^3; Phase view, France) and the values ranged between 0.26 μm and 0.88 μm and 0.52 μm and 0.90 μm, respectively. After wear testing, cross-sectional images were taken from four points of the circular wear track using the same 3D optical profilometer. The average of four area measurements was taken and the obtained value was

multiplied by the diameter of the circular track profile to calculate the volumetric wear loss for each specimen.

RESULTS AND DISCUSSION

Microstructure and XRD Analyses

Figure 1 shows the optical image and XRD pattern of the unmelted and remelted NiCrBSi flame spray coating. As seen in Fig. 1a, the microstructure contains a coating layer of about 1360 μm and an interlayer of about 60 μm, while the STKM-13A matrix below these layers were formed from the surface to the interior in the unremelted sample, respectively. In the remelted sample, the coating consists of about 1425 μm NiCrBSi and about 75 μm of an interlayer (Fig. 1b). Considering the morphology obtained, the flame-sprayed NiCrBSi coating shows a dense and homogeneous laminar structure
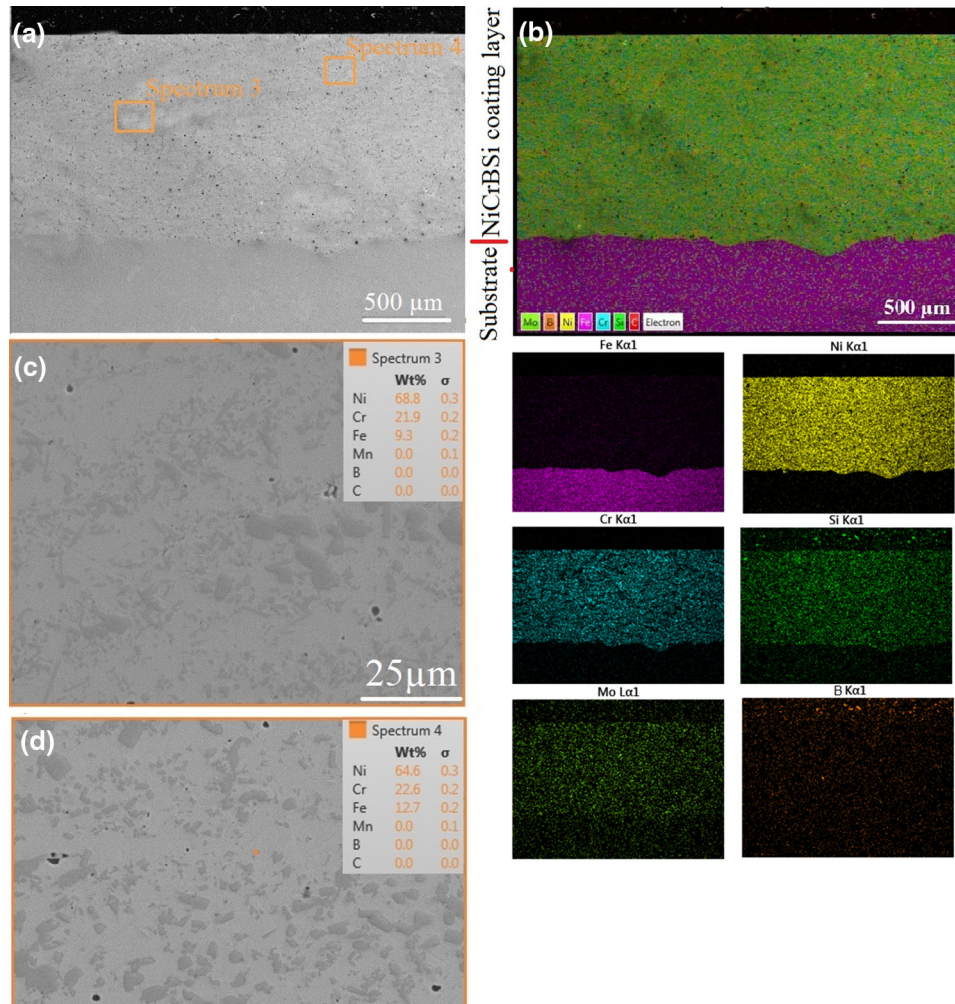

Fig. 2. (a) SEM view of NiCrBSi coated STKM-13A steel, (b) the distribution of elements according to EDS analysis, and elemental percent contents of (c) spectrum 3 and (d) spectrum 4.
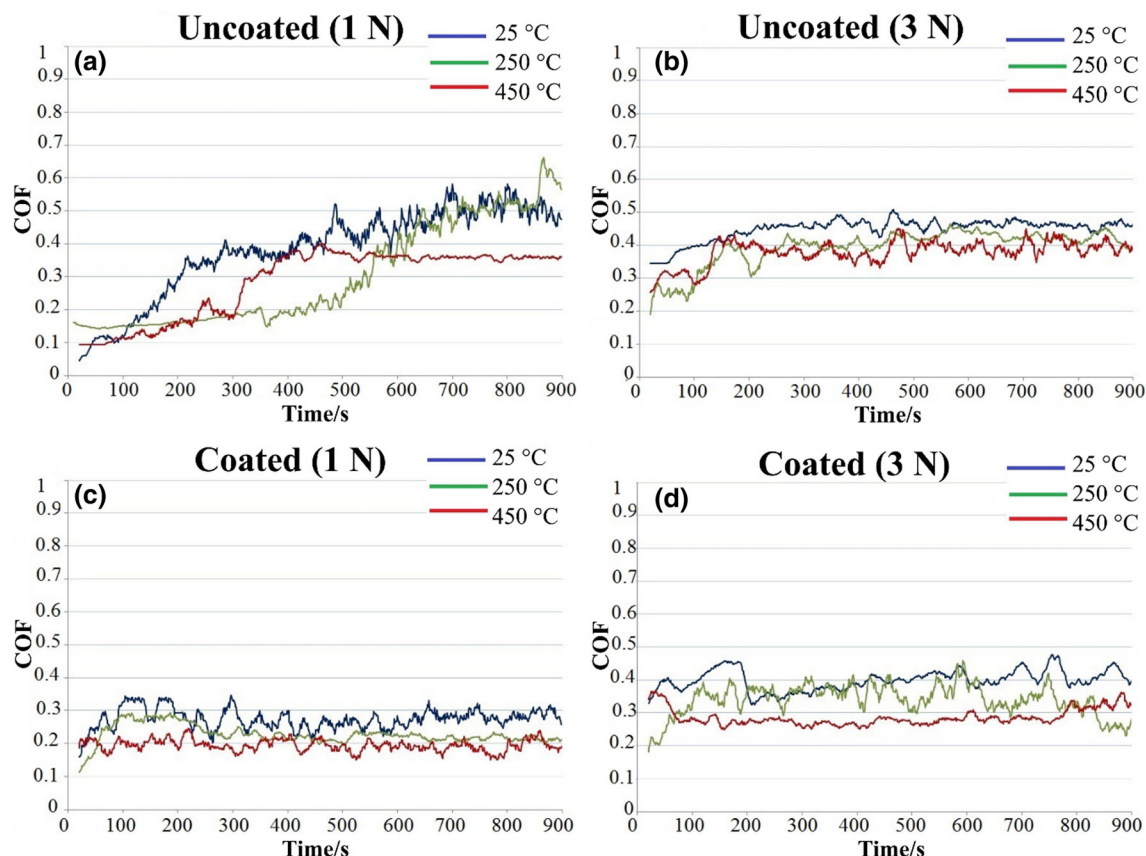
Fig. 3. The COFs over 900 s of testing for the un-coated specimens under (a) 1 N and (b) 3 N loading, and for the remelted NiCrBSi coated specimens under (c) 1 N and (d) 3 N loading.

and greater hardness values (965 ± 10 HV0.1) than the non-flame-sprayed sample (851 ± 20 HV0.1) (Fig. 1a and b).[6] The increase in the obtained hardness is due to the dispersion strengthening effect of the precipitates formed by the heat treatment.[20,27] On the other hand, the amount of porosity decreased from 8.9% to 2.3% in the remelting process. Although a significant amount of particles (about fourfold) were prevented from having low porosity, properties such as small pores and unmelted particles were observed in some regions in the coating (Fig. 1b), accepted as a natural characteristic of the TS methods. These properties are usually unwelcome as they can deteriorate the coating properties, especially adhesion strength, hardness, and wear and corrosion resistance, reported by many researchers.[25,29] The features resulting from flame spray method was eliminated by the subsequent remelting process (Fig. 1b). On the other hand, the specific properties of the phases determined by XRD analysis before and after remelting have been given in detail (see supplementary Table SI). The as-sprayed NiCrBSi coating layer formed on STKM-13A consisted mainly of Cr_2B and NiCr phases and a minor amount of $Cr_{23}C_6$ and Fe_3Ni (Fig. 1c).[6] As a result of the remelting process, Fe_3Ni was absent and instead it

was determined that Fe_2B was formed. In fact, these phases were also common for NiCrBSi alloy coatings prepared by flame spraying and other techniques such as plasma spray, HVOF, and laser cladding.[9,19,28,31]

The average thickness of the remelted flame-sprayed NiCrBSi coating layers was measured to be about 1.4 mm (Fig. 2a). Since the coating was quite thick, EDS mapping was carried out to examine whether the coating powder (Metco 15F) displayed any inhomogeneity (Fig. 2b). When Spectrum 3 and Spectrum 4 are compared, their chemical contents are approximately equal and included mainly Ni, Cr and Fe elements (Fig. 2c and d). B and Si are at low levels, and have a homogeneous distribution as with other elements in the EDS mapping (Fig. 2b). The hardness values (965 ± 10 $HV_{0.1}$) taken on the coating layer are close to each other, further supporting the fact that the elemental distribution is homogeneous.

Characterization of COF and Wear Profiles Microstructure

The COFs of uncoated and remelted NiCrBSi-coated specimens versus time are shown in Fig. 3, and the average COF values are given in Table I. In general, there was an increasing trend in the COFs

over time, recorded during the sliding of the uncoated specimens. On the other hand, the COFs obtained from the articulation of the coated samples commonly increased at the initial stage of testing (until the porous structure of the coated layer was removed), and then decreased. The decrease was because of the oxidation of the coating surface, which had a lubrication effect.[33,35,36] After 200 s of testing, the COFs of the coated samples were stabilized, which indicated that the coating retained its integrity throughout the wear test. This was supported by the depth measurements of the wear

traces (Fig. 4). Moreover, average COFs between 0 s and 900 s of testing decreased at lower applied loads and higher test temperatures. The decrease in the COFs at elevated temperatures was attributed to the formation of oxide layers on the specimens' surfaces, which may have caused a lubricative effect (Figs. 6 and 7).[33]

Figure 4 shows the wear traces and areas obtained from the worn surfaces of the uncoated and coated specimens at 25°C, 250°C and 450°C under 3-N loading. A V-shaped wear profile was observed for the uncoated samples, while a more complex V-shaped zone in which one next to and within the other for the coated samples. The complex V-shaped profile was attributed to the different wear characteristics of the phases formed at the coating layers (Fig. 1d), and to different mechanical properties from those of these phases at various test temperatures. For instance, the wear traces obtained from the coated and uncoated samples were found to be similar to each other for the experiments performed at room temperature, but they were considerably different at 250°C and 450°C (Figs. 6a and 7a).

Table I. The mean COF values of the un-coated and coated samples wear-tested at different loads and temperatures

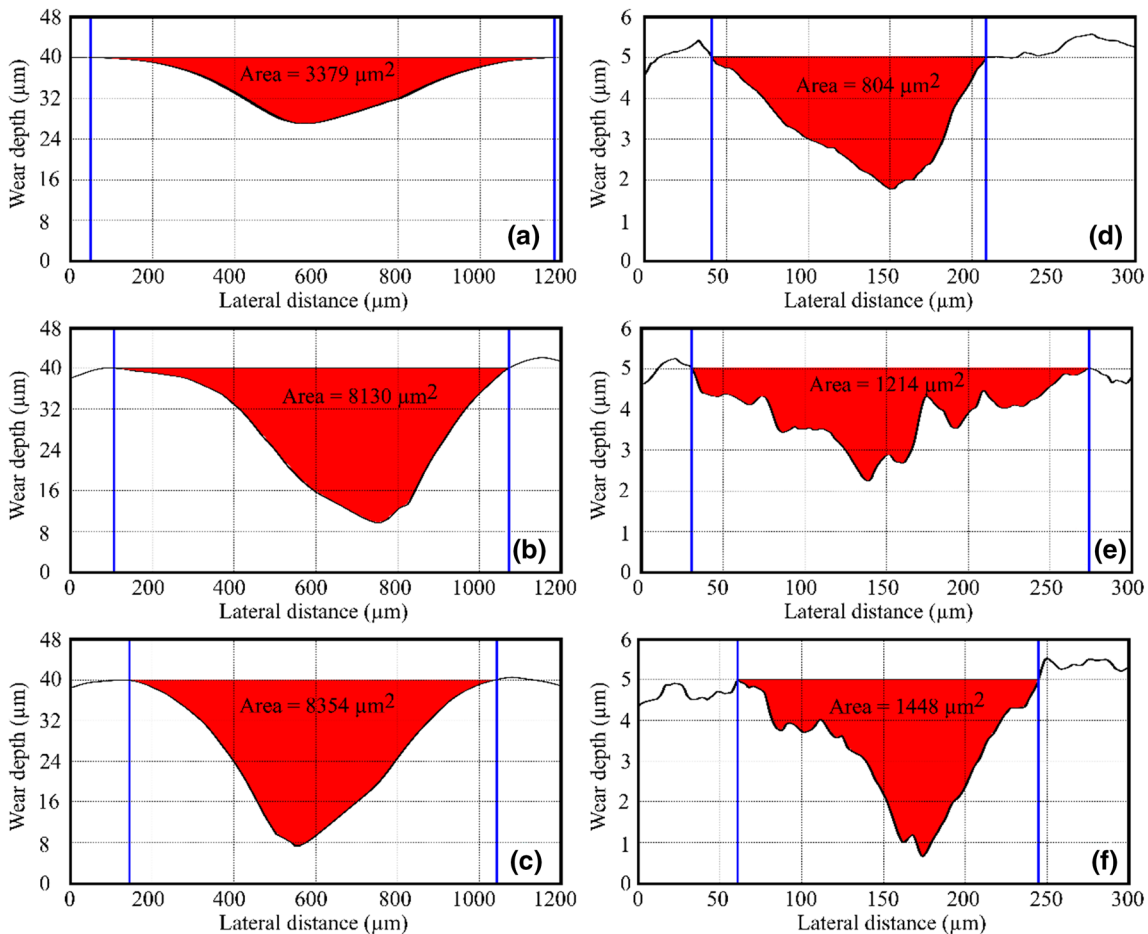| Sample	1 N			3 N		
	25°C	250°C	450°C	25°C	250°C	450°C
Uncoated	0.379	0.302	0.283	0.447	0.39	0.378
Coated	0.273	0.226	0.194	0.398	0.337	0.286

Fig. 4. The wear profiles and areas of the un-coated samples subjected to wear testing at (a) 25°C, (b) 250°C, (c) 450°C, and those of the coated samples tested at (d) 25°C, (e) 250°C, (f) 450°C under 3 N loading.
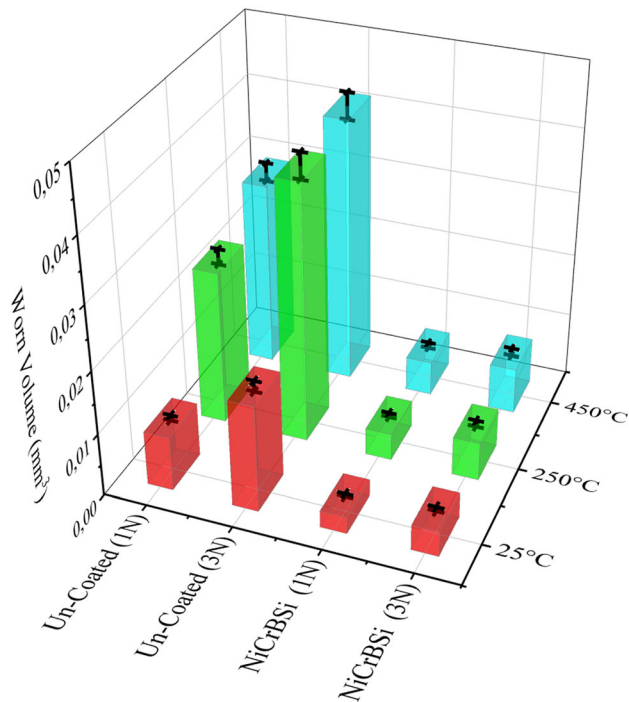
Fig. 5. The worn volume of the un-coated and coated specimens following wear testing, over various test temperatures and loads.

The wear volume changed considerably with the test temperature and applied load, as shown in Fig. 5. The coated samples showed superior wear resistance under all test conditions. Increasing the load from 1 N to 3 N did not result in a 3-fold increase in the volume loss. This suggests that strain hardening may have occurred during the wear testing.[37,38] In addition, under compressive loads, the pores and cracks present at the material surface are also sealed by microparticles, leading to densification. As a consequence of the formation of a denser and harder surface, the wear rate is reduced. Hence, strain hardening and densification caused by elevated loading resulted in increased surface hardness, which resulted in an increase in the wear resistance.[37]

The difference in wear rate between the coated and uncoated samples was much greater at higher temperatures. At 25°C, 250°C and 450°C, the volume losses of the coated samples were 69.2%, 82.5% and 81.4%, respectively, lower than those of the uncoated samples under 1 N, and they were 76.3%, 85.1% and 82.7%, respectively, lower under 3 N. Higher wear resistance at the elevated temperatures is attributed to the formation of the oxide layers.[33,35,36] During sliding, the surfaces are initially in contact at their asperities where a sudden temperature increase occurs,[39,40] which also accelerates oxide layer formation. The oxide layer provides lubrication, resulting in low COFs and volume losses.[33]

Wear Mechanisms

The characterization of the worn tracks provided ideas about the wear behaviors of the tested specimens. Thus, following wear experiments performed at different temperatures (25°C, 250°C, and 450°C), the wear tracks on the surfaces of the uncoated and flame-sprayed STKM-13A steel specimens were examined using SEM and EDS (Figs. 6 and 7).

The SEM images obtained from the surfaces of the uncoated specimens showed the presence of microcracks, wear particles, and wear protective layers (tribolayers) (Fig. 6). The tribolayer was first introduced to the literature in a study of nickel-based alloys by Jiang et al.[35] They observed a transition from severe to mild wear during dry sliding wear testing after some time of sliding.

Delamination wear caused by fatigue is the effective wear mechanism for the uncoated STKM-13A steel specimens (Fig. 6a). Tests performed at 250°C show microscratches, plastic deformation and extrusion zones along the sliding direction under high load (Fig. 6b). At 450°C, microcracks, extrusion zones, wear particles and tribolayers are present on the uncoated steel surfaces. These are caused by the compressive and tensile stresses that formed normal and parallel to sliding direction, respectively (Fig. 6c). Moreover, some wear debris is retained within the wear track at all test temperatures (Fig. 6). Although the worn surfaces of the uncoated specimens tested at 250°C and in particular at 450°C were found to be larger than those at room temperature, they were smoother, as observed in the SEM images. The WC ball and the STKM-13A steel sample initially came into contact at the asperities of the sliding surfaces. During wear testing, the wear particles were removed from the asperities of the STKM-13A steel samples and transferred between the two surfaces. After that, the particles were subjected to plastic deformation under the applied loads, and were retained within the wear tracks on the STKM-13A steel surfaces. The wear particles which were oxidized and thus hardened formed a temporary protective layer on the material surface; the test temperature had a substantial effect on the formation of the tribolayer.[35,41]

The SEM images of the remelted NiCrBSi samples subjected to wear testing at room temperature showed the presence of the cracks, microfractures, wear debris, and partial removal of the coating layer. The delamination wear mechanism was observed on the coated material surface, and the coating layer was spalled in some regions (Fig. 7a). The formation of the delamination mechanism has been described as having four stages: (1) plastic deformation in the surface layers under the effect of normal and tangential loads, (2) the nucleation of voids or cracks caused by deformation around the inclusions or the second phase particles, (3) the
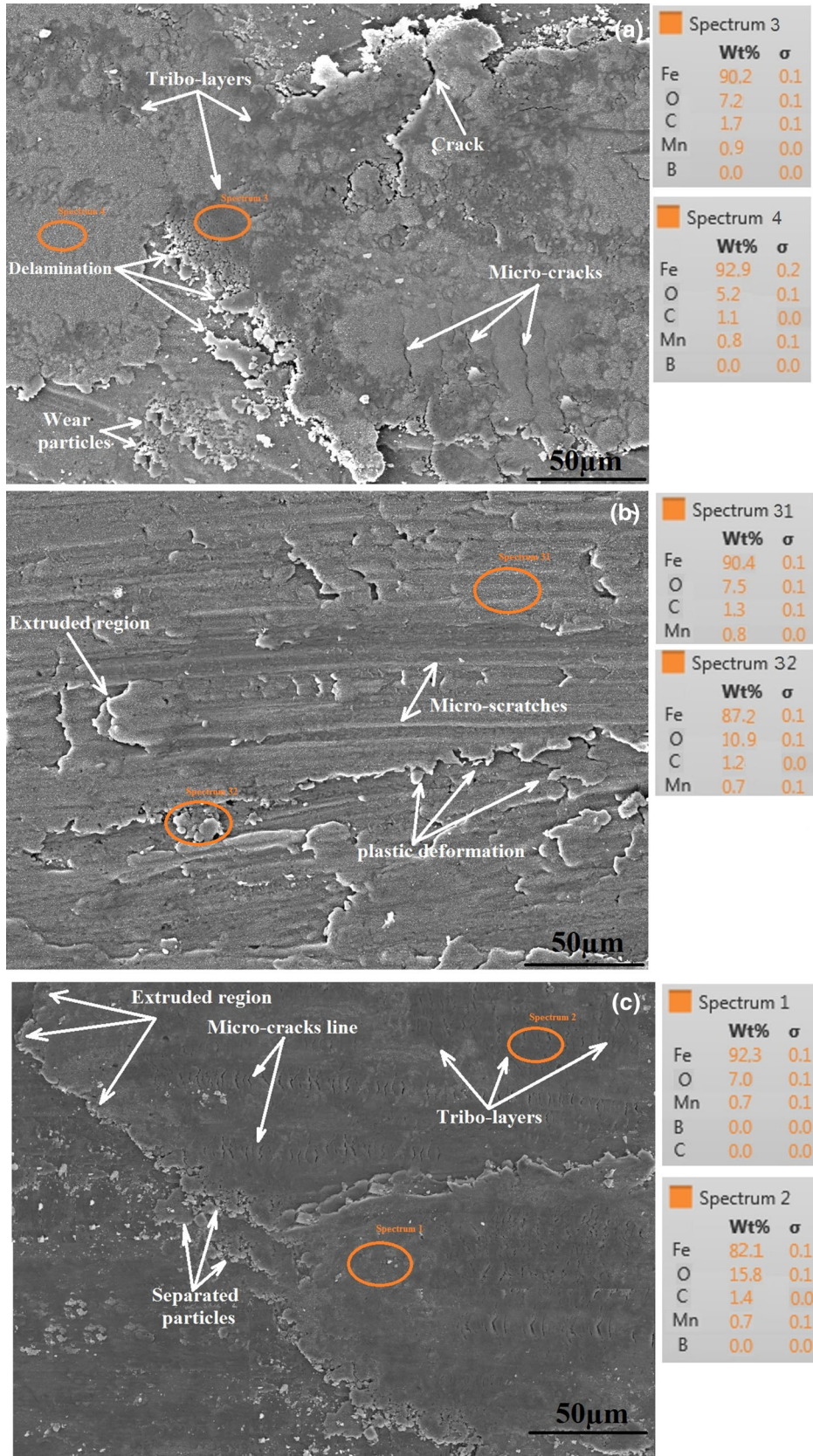
Fig. 6. The SEM image obtained from the surface of an un-coated STKM-13A steel specimen, wear-tested under 3 N loading, at 270 m sliding distance, (a) at room temperature (b) at 250°C temperature (c) at 450°C temperature.
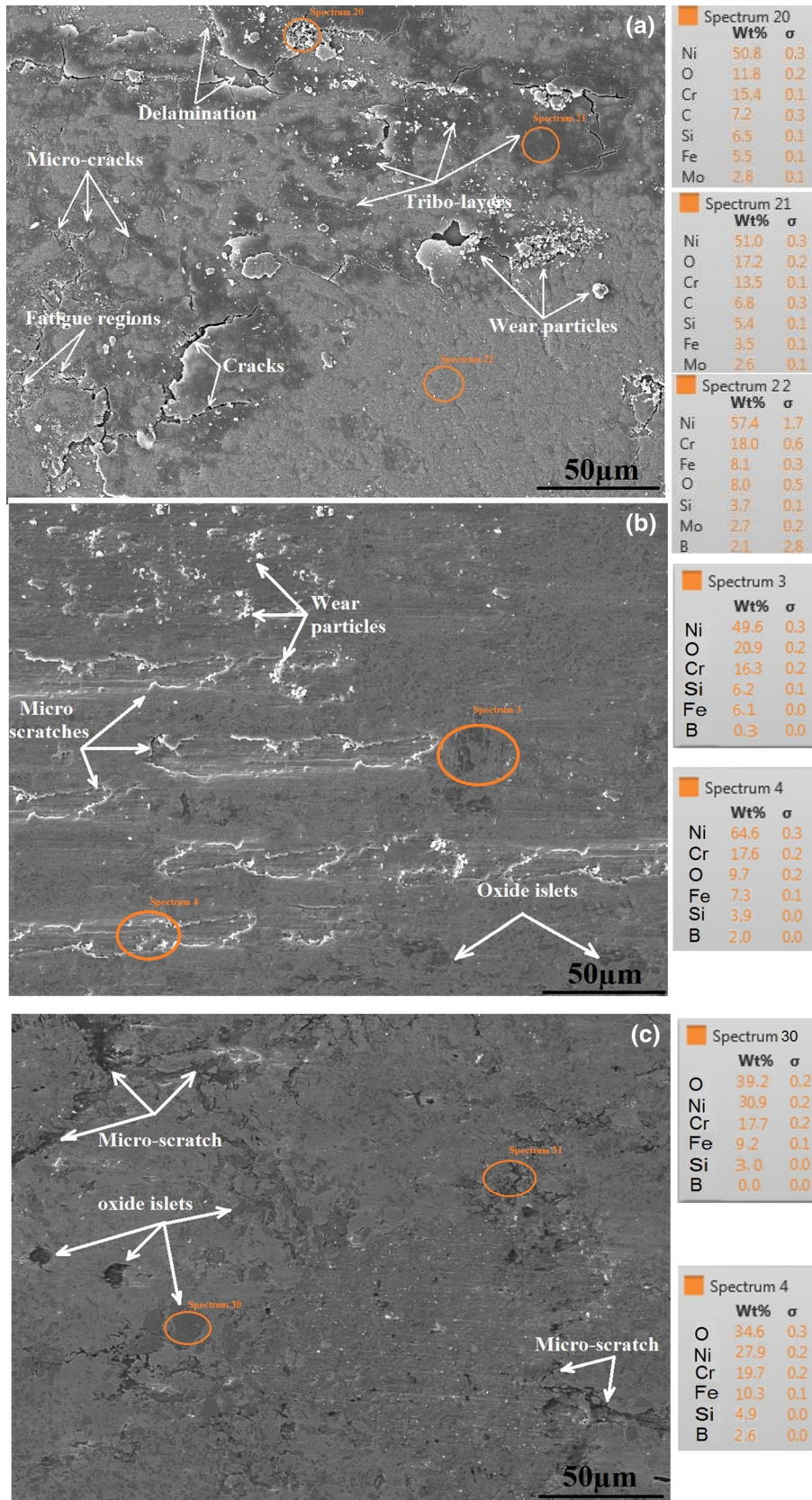
Fig. 7. The SEM image obtained from the surface of a remelted NiCrBSi coated, flame sprayed on STKM-13A steel specimen, wear-tested under 3 N loading, at 270 m sliding distance (a) at room temperature (b) at 250°C temperature (c) at 450°C temperature.

crack growth parallel to the material surface, and (4) the formation of thin and long wear particles and their removal from the material surface.[42,43] The surfaces of the remelted NiCrBSi specimens subjected to wear testing at 250°C and 450°C were found to be smoother than those tested at room temperature, which had only microscale scratches (Fig. 7b and c). The SEM images show that the oxide layer (or glaze) was more stable on the worn surfaces tested at the elevated temperatures, especially at 450°C.

Depending on the initiation and progression of the wear process, a glaze begins to form when wear particles are removed from the material surface due to the oxidation rate reaching a critical value. The layer forms as the micron-sized wear debris are retained within the wear tracks under repetitive loads and nominal pressures due to sintering.[36] The glaze layer forms a solid lubricant effect at high temperatures, and the solid lubricant reduces the shear forces which significantly affects the wear rate of a material.[44] The SEM images show that the dominant wear mechanism of the coated samples is delamination at room temperature, spalling, and adhesion as a consequence of extrusion at 250°C, and the oxidation at 450°C.

CONCLUSION

In this study, the friction and wear behavior of uncoated and remelted NiCrBSi flame-sprayed STKM-13A low alloy steel samples were compared under different applied loads and at different temperatures. From the experimental results, the following conclusions can be drawn:

1. The morphology of the NiCrBSi coating obtained was a compact homogeneous structure consisting mainly of Cr_2B and NiCr phases and a minor amount of $Cr_{23}C_6$ and Fe_2B.
2. Increasing the applied load increased the average COF values, but the increase in the wear test temperature reduced the average COFs due to the forming of the oxidation layer. The average COF values of the NiCrBSi coating at 25°C, 250°C, and 450°C were 0.273, 0.226, and 0.194 under 1 N and 0.398, 0.337, and 0.286 under 3 N, respectively. The mean COFs of uncoated STKM-13A were 0.379, 0.302, and 0.283 under 1 N and 0.447, 0.390, and 0.378 under 3 N, respectively.
3. Wear volumes for both the uncoated and coated specimens increased with increasing applied load and temperature. However, a 3-fold increase in load or temperature did not cause a 3-fold increase in the volume loss. The superior wear resistance of the coated sample at low temperatures was primarily due to strain hardening coupled with densification under elevated loads, and oxide formation at elevated temperatures.
4. The dominant wear mechanisms of the NiCrBSi-

coated specimen were delamination at room temperature, spalling due to extrusion at 250°C, and oxidation at 450°C. On the other hand, in the uncoated sample at room temperature, delamination was due to fatigue, and at 250°C and 450°C, microcracking and oxidation-type wear occurred.
5. Low-cost NiCrBSi-coated and -remelted specimens provided a superior wear and friction performance than the uncoated specimens under all test conditions, suggesting the application of NiCrBSi coatings in rolling mills running at high temperatures.

ELECTRONIC SUPPLEMENTARY MATERIAL

The online version of this article (https://doi.org/10.1007/s11837-019-03950-6) contains supplementary material, which is available to authorized users.

REFERENCES

1. W.L. Roberts, *Hot rolling of steel* (New York: Marcel Dekker, 1983), pp. 1–3.
2. R. Colás, J. Ramírez, I. Sandoval, J.C. Morales, and L.A. Leduc, *Wear* (1999). https://doi.org/10.1016/S0043-1648(99)00081-2.
3. C. Ould, X. Badiche, P. Montmitonnet, and Y. Gachon, *Wear* (2013). https://doi.org/10.1016/j.wear.2013.07.007.
4. J.D.B. De Mello, J.L. Gonçalves, and H.L. Costa, *Wear* (2013). https://doi.org/10.1016/j.wear.2013.02.006.
5. C. Ould, Y. Gachon, P. Montmitonnet, and X. Badiche, in *14th International Conference on Material Forming Esaform, Proceedings, Book Series: AIP Conference Proceedings,* (2011). https://doi.org/10.1063/1.3589768.
6. A. Günen, E. Kanca, M.S. Karakaş, V. Koç, M.S. Gök, A. Çürük, and M. Demir, Application of different coating methods to external cooling roller and characterization of applied coatings. in *3rd Iron and Steel Symposium (UDCS'17),* (2017), ISBN 978-605-9554-0-60.
7. V. Mayor, Applying traction coating to steel mill rolls, thermal spray: practical solutions for engineering problems. in *9th National Thermal Spray Conference & Exposition,* (1996) pp. 61–64.
8. C. Ould, X. Badiche, P. Montmitonnet, and Y. Gachon, *J. Manuf. Process.* (2013). https://doi.org/10.1016/j.jmapro.2012.09.011.
9. A. Ray, K.S. Arora, S. Lester, and M. Shome, *J. Mater. Process. Technol.* (2014). https://doi.org/10.1016/j.jmatprotec.2014.02.027.
10. G. Walmag and G. Esser, Work roll manufactured by laser cladding and method therefor, *Patent,* PCT/EP2015/073189, WO2016055545 A1 (2016).
11. S. Abraham, J.T. Ok, and K.H. Kim, *J. Mater. Process. Technol.* (2007). https://doi.org/10.1016/j.jmatprotec.2006.11.091.

12. H. Liang, F. Ma, X. Wang, T. Zhang, H. Zhu, X. Wu, and H. Zhang, *Surf. Coat. Technol.* (2000). https://doi.org/10.1016/S0257-8972(00)00625-3.
13. S. Matthews and B. James, *J. Therm. Spray Technol.* (2010). https://doi.org/10.1007/s11666-010-9518-8.
14. R. González, M.A. García, I. Peñuelas, M. Cadenas, M.D.R. Fernández, A.H. Battez, and D. Felgueroso, *Wear* (2007). https://doi.org/10.1016/j.wear.2007.01.094.
15. X.C. Zhang, B.S. Xu, S.T. Tu, F.Z. Xuan, Y.K. Zhang, H.D. Wang, and Y.X. Wu, *Fatigue Fract. Eng. Mater.* (2009). https://doi.org/10.1111/j.1460-2695.2008.01305.x.
16. J.R. Davis, *Handbook of Thermal Spray Technology* (Materials Park, OH: ASM International, 2004), pp. 41–82.
17. R.C. Tucker, eds., *Thermal Spray Technology*, Vol. 5A (Materials Park: ASM Handbook, 2013), pp. 75–125.
18. T. Gómez-del Río, M.A. Garrido, J.E. Fernández, M. Cadenas, and J. Rodríguez, *J. Mater. Process. Technol.* (2008). https://doi.org/10.1016/j.jmatprotec.2007.11.042.
19. M.A. Garrido, A. Rico, M.T. Gómez, M. Cadenas, J.E. Fernández-Rico, and J. Rodríguez, *J. Therm. Spray Technol.* (2017). https://doi.org/10.1007/s11666-016-0521-6.
20. B. Liang, Z. Zhang, and H. Guo, *Trans. Indian Inst. Met.* (2017). https://doi.org/10.1007/s12666-016-1014-5.
21. J. Rodríguez, A. Martín, R. Fernández, and J.E. Fernández, *Wear* (2003). https://doi.org/10.1016/S0043-1648(03)00162-5.
22. R. González, M. Cadenas, R. Fernández, J.L. Cortizo, and E. Rodríguez, *Wear* (2007). https://doi.org/10.1016/j.wear.2006.05.009.
23. Š. Houdková, E. Smazalová, M. Vostřák, and J. Schubert, *Surf. Coat. Technol.* (2014). https://doi.org/10.1016/j.surfcoat.2014.05.009.
24. J.M. Miguel, J.M. Guilemany, and S. Vizcaino, *Tribol. Int.* (2003). https://doi.org/10.1016/S0301-679X(02)00144-5.
25. Z. Bergant and J. Grum, *J. Therm. Spray Technol.* (2009). https://doi.org/10.1007/s11666-009-9304-7.
26. M.R. Karimi, H.R. Salimijazi, and M.A. Golozar, *Surf. Eng.* (2016). https://doi.org/10.1179/1743294415Y.0000000107.
27. K. Simunovic, L. Slokar, and S. Havrlisan, *Philos. Mag.* (2017). https://doi.org/10.1080/14786435.2016.1257167.
28. E.E. Kornienko, A.A. Nikulina, N.S. Belousova, D.V. Lazurenko, A.S. Ivashutenko, and V.I. Kuz'min, in *IOP Conference Series: Materials Science and Engineering* (2016). https://doi.org/10.1088/1757-899X/156/1/012020.
29. D. Chaliampalias, G. Vourlias, E. Pavlidou, S. Skolianos, K. Chrissafis, and G. Stergioudis, *Appl. Surf. Sci.* (2009). https://doi.org/10.1016/j.apsusc.2008.10.006.
30. A. Martín, J. Rodríguez, J.E. Fernández, and R. Vijande, *Wear* (2001). https://doi.org/10.1016/S0043-1648(01)00703-7.
31. K. Dejun and Z. Benguo, *Surf. Rev. Lett.* (2017). https://doi.org/10.1142/S0218625X17500573.
32. C. Guo, J. Zhou, J. Chen, J. Zhao, Y. Yu, and H. Zhou, *Wear* (2011). https://doi.org/10.1016/j.wear.2011.01.003.
33. A. Günen, E. Kanca, M.S. Karakaş, V. Koç, M.S. Gök, Y. Kanca, A. Çürük, and M. Demir, *Surf Coat. Technol.* (2018). https://doi.org/10.1016/j.surfcoat.2018.04.071.
34. A. Günen, B. Kurt, P. Milner, and M.S. Gök, *Int. J. Refract. Met. Hard* (2019). https://doi.org/10.1016/j.ijrmhm.2019.03.019.
35. J.R. Jiang, F.H. Stott, and M.M. Stack, *Wear* (1995). https://doi.org/10.1016/0043-1648(95)90004-7.
36. P.W. Stott, A.C. Williams, and B.W. Barry, *J. Control. Release* (1998). https://doi.org/10.1016/S0168-3659(97)00153-3.
37. L.C. Betancourt-Dougherty and R.W. Smith, *Wear* (1998). https://doi.org/10.1016/S0043-1648(97)00212-3.
38. R. Tyagi, D. Xionga, and J. Li, *Wear* (2011). https://doi.org/10.1016/j.wear.2010.08.013.
39. J.F. Archard, *J. Appl. Phys.* (1953). https://doi.org/10.1063/1.1721448.
40. M. Woydt and K.H. Habig, *Tribol. Int.* (1989). https://doi.org/10.1016/0301-679X(89)90168-0.
41. H. Engqvist, H. Högberg, G.A. Botton, S. Ederyd, and N. Axén, *Wear* (2000). https://doi.org/10.1016/S0043-1648(00)00315-X.
42. N.P. Suh, *Wear* (1973). https://doi.org/10.1016/0043-1648(73)90125-7.
43. K. Kato, *Tribol. Int.* (1997). https://doi.org/10.1016/S0301-679X(96)00063-1.
44. H.A. Sodano, J.M. Lloyd, and D.J. Inman, *Adv Mater Res-Switz.* (2006). https://doi.org/10.1088/0964-1726/15/5/007.